ISSN 1674-1056
http://cpb.iphy.ac.cn
http://iopscience.iop.org/cpb
中国物理 B
Chinese Physics
中国物理
Chinese Physics B

Spin manipulation in semiconductor quantum dots qubit

Ke Wang(王柯), Hai-Ou Li(李海欧), Ming Xiao(肖明), Gang Cao(曹刚), Guo-Ping Guo(郭国平)

Citation: Chin. Phys. B . 2018, 27(9): 090308. **doi:** 10.1088/1674-1056/27/9/090308

Journal homepage: http://cpb.iphy.ac.cn; http://iopscience.iop.org/cpb

What follows is a list of articles you may be interested in

Qubits based on semiconductor quantum dots

Xin Zhang(张鑫), Hai-Ou Li(李海欧), Ke Wang(王柯), Gang Cao(曹刚), Ming Xiao(肖明), Guo-Ping Guo(郭国平)

Chin. Phys. B . 2018, 27(2): 020305. **doi:** 10.1088/1674-1056/27/2/020305

Invariants-based shortcuts for fast generating Greenberger—Horne—Zeilinger state among three superconducting qubits

Jing Xu(徐晶), Lin Yu(于琳), Jin-Lei Wu(吴金雷), Xin Ji(计新)

Chin. Phys. B . 2017, 26(9): 090301. **doi:** 10.1088/1674-1056/26/9/090301

Fast generating *W* state of three superconducting qubits via Lewis-Riesenfeld invariants

Lin Yu(于琳), Jing Xu(徐晶), Jin-Lei Wu(吴金雷), Xin Ji(计新)

Chin. Phys. B . 2017, 26(6): 060306. **doi:** 10.1088/1674-1056/26/6/060306

Dynamical decoupling pulses on the quantum correlations for the system of superconducting quantum circuit

Wang Dong-Mei, Qian Yi, Xu Jing-Bo, Yu You-Hong

Chin. Phys. B . 2015, 24(11): 110304. **doi:** 10.1088/1674-1056/24/11/110304

Geometric quantum discord and Berry phase between two charge qubits coupled by a quantum transmission line

Zhu Han-Jie, Zhang Guo-Feng

Chin. Phys. B . 2014, 23(12): 120306. **doi:** 10.1088/1674-1056/23/12/120306

TOPICAL REVIEW — Spin manipulation in solids

Spin manipulation in semiconductor quantum dots qubit*

Ke Wang(王柯), Hai-Ou Li(李海欧), Ming Xiao(肖明),
Gang Cao(曹刚)†, and Guo-Ping Guo(郭国平)‡

CAS Key Laboratory of Quantum Information, University of Science and Technology of China, Hefei 230026, *China*

(Received 19 May 2018; revised manuscript received 18 June 2018; published online 28 August 2018)

Thirty years of effort in semiconductor quantum dots has resulted in significant developments in the control of spin quantum bits (qubits). The natural two-energy level of spin states provides a path toward quantum information processing. In particular, the experimental implementation of spin control with high fidelity provides the possibility of realizing quantum computing. In this review, we will discuss the basic elements of spin qubits in semiconductor quantum dots and summarize some important experiments that have demonstrated the direct manipulation of spin states with an applied electric field and/or magnetic field. The results of recent experiments on spin qubits reveal a bright future for quantum information processing.

Keywords: semiconductor quantum dot, qubits, spin, manipulation

PACS: 03.67.Lx, 68.65.–k, 71.70.Ej, 78.67.Hc **DOI:** 10.1088/1674-1056/27/9/090308

1. Introduction

The field of quantum information technology is rapidly developing, and scientists are actively trying to implement efficient quantum gates in a variety of systems, particularly in solid-state systems. Manipulating spin states in semiconductors is one of the most important avenues for constructing a quantum gate, considering that electron spin is a reliable carrier of processed information and can be manipulated arbitrarily with a relatively high reliability. The realization of electrical or magnetic control of spin states in semiconductors has provided compelling evidence of the potential computing applications.

Nearly three decades ago, research was initiated on quantum dots which were known as artificial atoms.[1–3] In the beginning, the exact number of electrons in the dots was uncertain. The precise number was eventually confirmed in 1996.[4] Shortly thereafter, the proposal for a quantum computer architecture using electron spins in quantum dots (QDs) was developed. Later, the precise control of spin states was demonstrated via electrical methods.[5] After a series of successful experiments, scientists were able to characterize these systems based on several parameters including T_1 (relaxation time) and T_2 (coherence time). At the same time, the Pauli spin blockade phenomenon was discovered in double quantum dots (DQDs).[6] At present, one of the spin-to-charge conversion strategies based on this phenomenon is widely used to initialize and readout the spin states of electrons in QDs.[7]

The first demonstration of electrically controlled single-spin qubits was reported in 2005.[8] Several years later, two-spin qubits were realized as well as the entanglement of the encoded spin states in GaAs QDs.[9,10] In addition, single-spin qubits and two-spin qubits are implemented in silicon metal–oxide semiconductor (Si MOS)[11–13] and Si/SiGe systems.[14–18] Currently, it is possible to achieve a gate fidelity of 90% for different systems and occasionally, even higher than 99%.[19–21] However, further research is still required to improve the coherence time and fidelity.

This section summarizes the status of research in spin qubits in a semiconductor quantum dot. Section 2 is an introduction to the main concepts of QDs including a discussion of the basic properties and detection of double quantum dots. The methods for readout will be discussed in sections 3 and 4. Section 5 is a review of spin qubits, and the effect of the environmental influence will be highlighted in section 6. Section 7 will summarize the manipulation methods of spin states and discuss the details of each method. Finally, section 8 is the outlook and conclusion.

2. Developments and electronic properties of gate-defined quantum dots

2.1. Evolution of semiconductor quantum dots

A quantum dot is a kind of 'artificial atom.' It can be filled with electrons (or holes) confined by a certain metal gates structure. The dot is coupled with reservoirs via tunnel barriers and can be detected by applying a current and/or voltage. Also, it is capacitively coupled to gates. By changing

*Project supported by the National Key R&D Program of China (Grant No. 2016YFA0301700), the National Natural Science Foundation of China (Grant Nos. 11674300, 61674132, 11575172, and 11625419), and the Fundamental Research Fund for the Central Universities, China.

†Corresponding author. E-mail: gcao@ustc.edu.cn

‡Corresponding author. E-mail: gpguo@ustc.edu.cn

© 2018 Chinese Physical Society and IOP Publishing Ltd

the gate voltage, the electrostatic potential can be tuned, and properties of the dots can be controlled. The structures of typical lateral and vertical quantum dots are shown in Figs. 1(a) and 1(b), respectively.

The initial focus of the application of quantum dots is for device fabrication on GaAs/AlGaAs heterostructures.[19] In addition to the rapid improvement in technology, high mobility GaAs/AlGaAs heterostructures, Si/SiGe heterostructures,[20–22] Si-MOS,[23–25] graphene,[26–30] and other novel materials[31–36] have also been employed as host materials. It should also be noted that the research focus has transitioned from doped heterostructures to undoped heterostructures,[37–41] since the coherence of spin states is affected by the dopants around the electrons. Nuclear spin plays an important role in the coherence of spin states. At present, purified silicon is regarded as an excellent candidate for spin qubits due to the absence of nuclear spins.[42,43]

The structure of quantum dots changes significantly. Figure 1(c) shows the lateral structure using doped heterostructures. There is also another accumulating-gate structure with undoped heterostructures.[44–46] Overlapping-gates have been invented to define quantum dots with smaller sizes over the last few years.[47] These changes are aimed at defining quantum dots with smaller sizes in larger quantities. As such, it may be possible to accomplish more complex operations on chips.

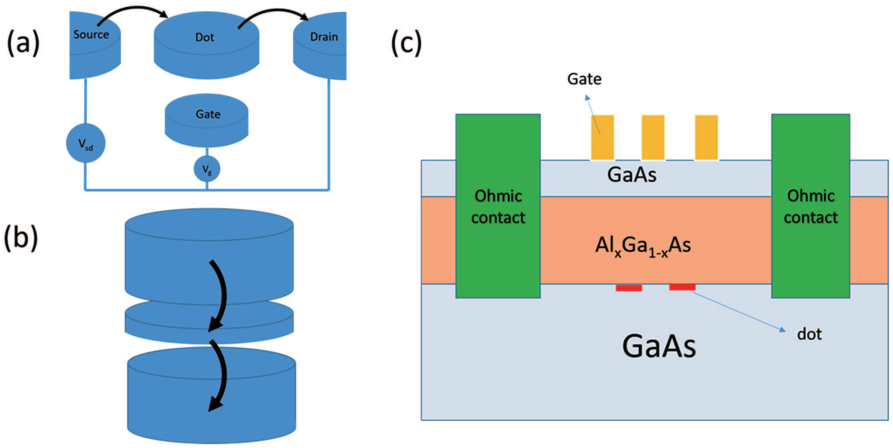


Fig. 1. (color online) Schematic diagrams of (a) lateral dot and (b) vertical dot, (c) vertical dots fabricated on a GaAs heterostructure.

2.2. Electronic properties of electrons in double quantum dots

Taking a double quantum dot as an example, if we ignore the spin of an electron, the charge stability diagram (so-called honeycomb diagram) shown in Fig. 2 can be used to describe the electronic properties of double quantum dots. Usually, the coupling between double quantum dots is considered as $C_m > 0$, and $V_{G,1}$, $V_{G,2}$ represent the gate voltage on the gates which control dot 1 and dot 2, respectively. (m,n) which corresponds to the numbers of electrons in the dots as n (m), is the electron number in dot 1 (2), also written as a left dot (right dot) in the following section.[48]

Two effects dominate the electronic properties of quantum dots. One is the Coulomb repulsion between the electrons in the dots, which results in additional energy cost for adding one more electron. This leads to a Coulomb blockade in quantum dots. Another effect is the confinement of dots that leads to the discrete energy spectrum. As shown in Fig. 2(c), an additional electron can only occupy the vacant level between the Fermi levels of the source and drain.

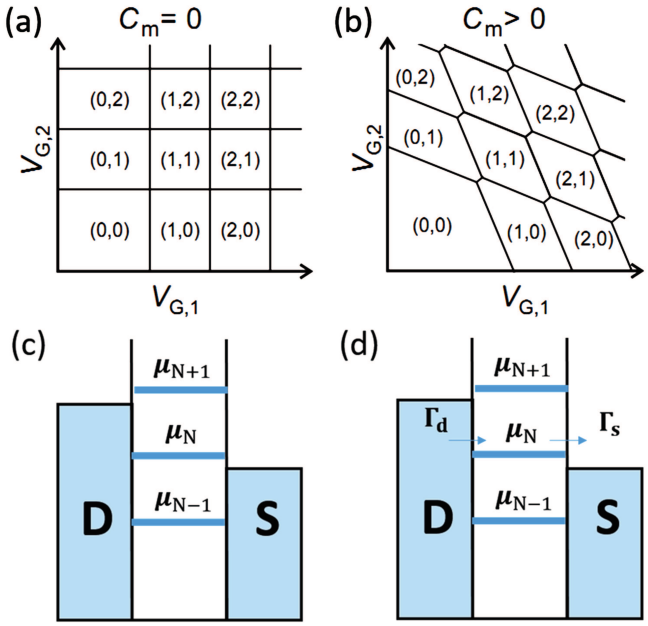


Fig. 2. (color online) Charge stability diagram of double quantum dots acquired by scanning $V_{G,1}$, $V_{G,2}$. (a) Uncoupled and (b) coupled quantum dots can be transformed reversibly into each other by tuning C_m. C_m is the cross capacitance between the dots. The lines in the diagram are the current signals while sweeping the voltage. (c) Discrete energy level of quantum dots (orbital states). (d) An electron can tunnel in (or out) of the dot with a rate Γ_s (or Γ_d). Panels (a) and (b) are from Ref. [48].

To understand these properties more clearly, it is necessary to investigate the dots with an appropriate measurement method. There are two traditional ways to obtain information. They include dc transport and charge sensing including quantum point contact (QPC) transport measurement and QPC modulation measurement.

2.3. Transport measurement

Transport measurement is the most direct method to reproduce a charge stability diagram. In this process, a dc bias and ammeters are directly linked to reservoirs of the double quantum dots (source and drain). Using the dc transport signal, $I_{\rm Dot}$, a triangle-shaped stability diagram (Fig. 4) is determined from Fig. 3. Certain parameters of these systems could be extracted from the triangles, especially in systems like nanowires, in which the signal is clear enough.[49–52]

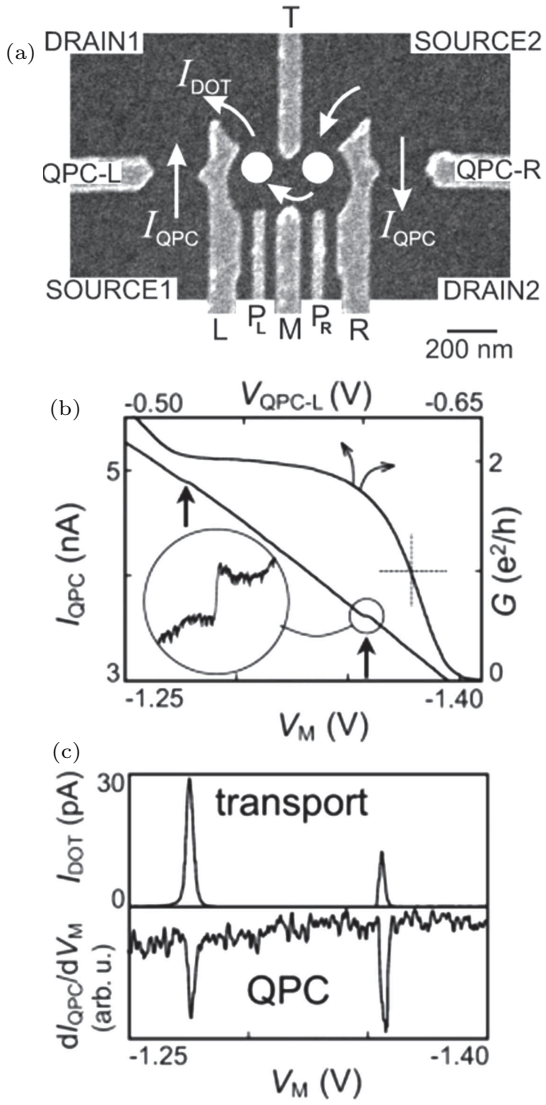


Fig. 3. (a) Measurement setup for transport and charge sensing. (b) The upper right curve is the QPC conductance versus the QPC gate voltage while the cross indicates the highly sensitive position. The lower left one is the transport signal of the QPC versus gate voltage $V_{\rm M}$. (c) The upper curve represents the transport signal of the double quantum dots, and the lower one indicates the modulation signal of the QPC. The figure is from Ref. [53].

2.4. Charge sensing technique

In addition to transport measurement, there is another method called charge sensing.[54] Superior to standard transport measurement, charge sensing techniques can be used to confirm the number of electrons in single[55] or double quantum dots[53] and to extract some key parameters such as detuning ε and inter-dot coupling $2t$.[56–61] In addition, due to the high sensitivity of charge sensors, charge sensing can be used in the absence of a transport signal or for the devices with only one reservoir.[62]

A charge sensor is formed by integrating the QPC beside the quantum dots. In Fig. 3, there are two QPCs in this device. This type of sensor can be used to detect information in two ways. One way is by measuring the transport signal of the QPC. It reflects the charge distribution at a fixed total charge. The QPC sensor is most sensitive to the tunneling of electrons in the steepest position (at $G \approx e^2/h$) between two plateaus of G.[63] Figure 3(b) shows the QPC transport current, where each plateau of $I_{\rm QPC}$ corresponds to an electron hopping event. The other way is by measuring the modulation signals. When a modulation or pulse signal is added to the gate which controls the electron behavior, the QPC sensor can obtain information with a high signal-to-noise ratio (SNR). Even when the transport current, $I_{\rm Dot}$, through the dot has fallen below the noise level, this modulation conductance variation still can be detected to confirm the change of the electron number. This is why the QPC can be used to confirm the number of electron in the dots. Compared to the transport current in double quantum dots in the upper panel of Fig. 3(c), the modulation signals agree well with it. Such a technique is widely used in GaAs quantum dot systems.[56,59,61] Single electron transistors (SETs) were also fabricated as an electrometer. They were first used in a resonant circuit operating at a frequency above 100 MHz.[64] SETs have been integrated into quantum dots and in various structure such as carbon nanotubes,[65–69] Ge/Si core-shell nanowires,[70] graphene[71,72] and Si MOSFETs.[73]

It is notable that charge sensing greatly depends on the tunneling rates (Γ). If the tunneling time ($1/\Gamma$) is much longer than the measurement time, no signal can be detected. In this case, the change of the electron number cannot be observed while sweeping the gate voltage. On the other hand, this phenomenon can be used to detect the tunneling time by adding short gate voltage pulses which draw electrons in and out. If the gate pulse amplitude is suitable, it can change the electrochemical potential and control the electron number to fluctuate between N and $N-1$. Monitoring the average current of the dot electron versus the length of the gate pulse yields information on the tunneling time. When the pulse length is comparable to the tunneling time, the average current of the electrons is sensitive to the change of the tunneling rate. So it can be used to measure the charge dynamics in GaAs quantum

dots.[61] It has also been used to measure the spin lifetime of a single electron in Si/SiGe[57,74] and Si-MOS quantum dots.[75]

In addition, two pulses simultaneously added to different gates are used to detect the spin states using a charge sensing technique.[76,77] Finally, improved readout of the spin states mediated by a metastable charge state has been developed, which aids the signal enhancement.[78,79]

3. Pauli spin blockade

The Pauli spin blockade (PSB) plays an important role in spin dynamics in quantum dots as indicated by the current suppression. The key point is that one orbital state can only be occupied by two electrons with different spin (so-called Pauli exclusion principle). As illustrated in Fig. 4, the PSB occurs when a negative source–drain bias is added. At a negative bias, the electron state transits in the sequence (0, 1)→(1, 1)→(0, 2)→(0, 1). There is always an electron in the right dot. Due to the Pauli exclusion principle, only a spin-down electron from the left dot can be loaded into the right dot during the transition (1, 1)→(0, 2) if the electron in the right dot is in the spin-up state. Similarly, only another spin-up electron can transition into the right dot if the first one is in the spin-down state. Using transport measurement, triangles which indicate current signals can be mapped out, as illustrated in Fig. 4. When each dot is occupied by one electron respectively, current suppression occurs during the transition (1, 1)→(0, 2), shown in Figs. 4(b) and 4(d). This is because of the energy difference between $S(0,2) = \frac{|\uparrow\downarrow\rangle - |\downarrow\uparrow\rangle}{\sqrt{2}}$ and $T(0,2) = |\uparrow\uparrow\rangle$ (arrows indicate the spin direction of electrons) is so large that the energy level of the $T(0,2)$ is above the Fermi level of the reservoir, as shown in Fig. 5(a).

On the contrary, for a positive bias, charge transfer takes place in the sequence (0, 1)→(0, 2)→(1, 1)→(0, 1). The first electron in the right dot is either spin-up or spin-down, and the second electron with an opposite spin direction can tunnel through the right dot, leading to an observable current. This is because the orbital states of each dot in the (1,1) regime are different and the splitting between $S(1,1)$ and $T(1,1)$ is comparatively small in the absence of the Pauli exclusion principle.

To clarify current suppression, a typical situation (negative bias) is considered. With an appropriate gate voltage, the (1, 1) regime can be reached. In this regime, each dot is occupied by one electron. Assuming a spin-up electron in the right dot is prepared as shown in Fig. 5(a), another electron hopping to the left dot from the drain can be either spin-up or spin-down. A spin-up electron can tunnel to the right dot while a spin-down electron cannot, as illustrated in Figs. 5(b) and 5(c). In the situation shown in Fig. 5(c), no additional current can be measured, since no charge transition occurs. This is why current suppression takes place.

The first PSB of quantum dots was observed in an experiment on vertical double quantum dots[6] and then in lateral quantum dots.[59] Mostly, this spin-to-charge phenomenon occurs in a two-electron regime, but it has been discussed in a three-electron regime as well.[80]

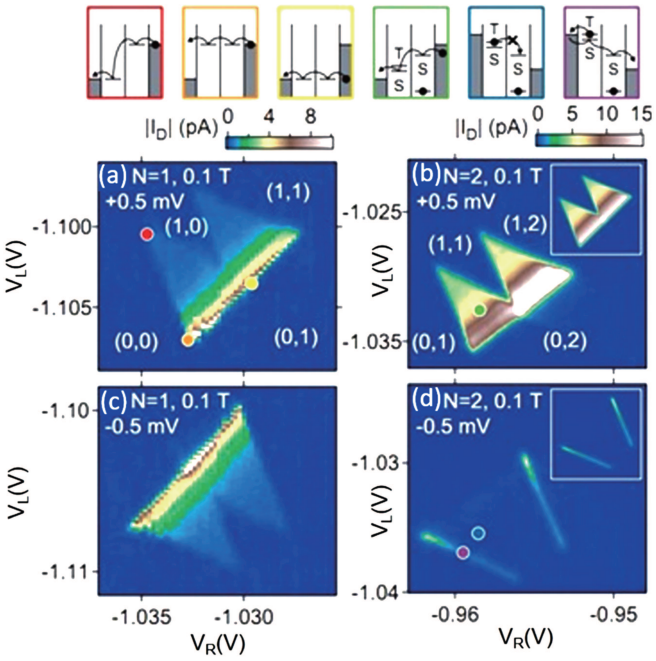


Fig. 4. (color online) The dc transport measured current by sweeping V_R and V_L with a (a), (b) positive bias and (c), (d) negative bias. (a), (c) In the one-electron regime, no spin blockade phenomenon is observed, (b), (d) while it is obvious in the two-electron regime. The figure comes from Ref. [59].

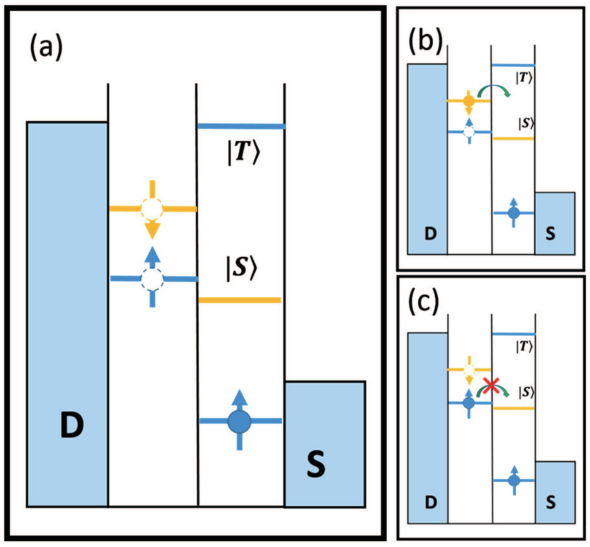


Fig. 5. (color online) Schematics of electrochemical potential. (a) Initial state of double quantum dots. Each dot is occupied by one electron and the electron in the right dot is spin-up while the state of the left electron is uncertain. Panels (b) and (c) represent two different situations. When a spin-down electron transits to a dot, it can transfer to the right one without restriction. However, a spin-up electron is forbidden from crossing due to the Pauli spin blockade.

4. Readout of spin states

4.1. Single-shot readout of electron spins

Due to the tiny magnetic moment of the electron spin, it is difficult to measure the spin state directly. Thus, a spin-to-charge conversion is needed to distinguish a single spin. Over the course of numerous experiments, two methods have been utilized for the readout stage. One is the energy selective readout (E-RO), where the energy difference between the different spin states should be large enough to distinguish a single spin.[7] The other is tunneling rate selective readout (TR-RO).[81] By exploiting the different tunneling rates between two spin states, spin-to-charge conversion is achieved. These two approaches are both important for possible applications in experiments. In both circumstances, the readout fidelities are above 99%.[82] Such strategies are not only suitable for a single spin, but also for two-spin states. Later, spin-state detection of two individual electrons is demonstrated using two independent QPC detectors at the same time.[83]

4.2. Energy selective readout

The first energy selective readout experiment was demonstrated in 2004.[7] As previously indicated, QPC works as an electrometer. When Zeeman splitting is much larger than the energy level broadening, E-RO can be achieved. In Fig. 6, the measurement consists of three steps: 1) empty the dot; 2) inject an electron with unknown spin; 3) measure the state. These steps are controlled by gate voltage pulse applied to the quantum dots in a finite magnetic field. Firstly, the dot should be empty which means both the spin-up and spin-down energy level are above the reservoir. Secondly, the gate pulse changes the energy until these two energy levels are below the reservoir. It should be mentioned here that the time interval of this process is approximating Γ^{-1}. Then only one electron can tunnel into the dot with either the spin-up or spin-down state. Finally, the pulse pulls the energy again, and the Fermi level of the reservoir is between the energy levels of the spin-up and spin-down state. Only the electron with a spin-down state can tunnel out of the dot because its energy is above $\mu_{\rm res}$. Therefore, an additional current step can be observed. At the end of the $t_{\rm read}$, the pulse ends and the empty stage starts again. In this way, spin-up and spin-down states can be detected in real time. Figures 6(c) and 6(d) are the experiment data.

4.3. Tunneling rate selective readout

The method mentioned here depends on the difference of the tunneling rates of the different spin states. The first demonstration of this technique was an experiment for the singlet state ($|S\rangle$) and the triplet state ($|T_0\rangle$).[81] Similar to the E-RO method, a gate pulse is needed to realize the three steps of measurement. Here we assume that the tunneling rate Γ_T from the $|T\rangle$ state to the reservoir is much larger than Γ_S from the $|S\rangle$ state. For dots with more than two electrons, it is possible to acquire different tunneling rates because the triplet state is asymmetric and the wave function of the triplet state is more extended than that of the singlet state, leading to a larger overlap with the reservoir.

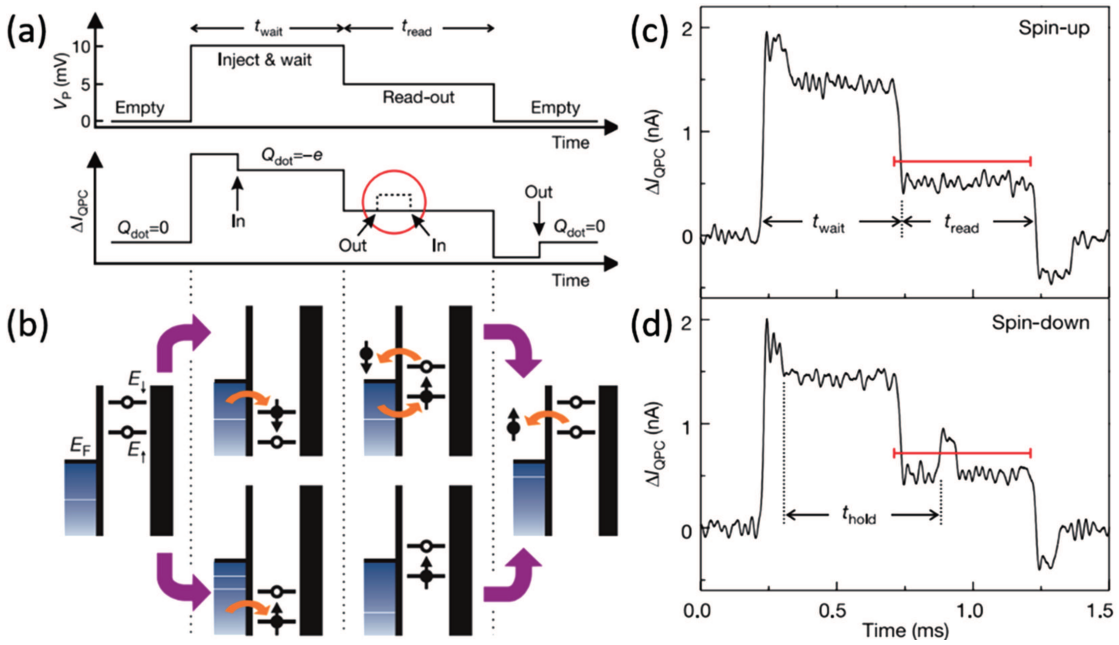


Fig. 6. (color online) Schematic diagrams of the E-RO single-shot readout progress. (a) The upper panel shows the gate voltage pulse, which consists of three steps: empty, inject & wait, and readout. The lower panel shows the response of the QPC signals. The dashed line represents the signal when spin-down is injected in. (b) Energy diagrams for spin-up and spin-down states for the different situations during the three pulse steps. The upper panel is a spin-down injected diagram while the lower one is spin-up injected. Panels (c) and (d) represent the experimental result of a single-shot readout of an electron spin for two different types of spin states: the upper panel corresponds to a spin-up electron and the lower panel is a spin-down electron. The figure comes from Ref. [7].

Like E-RO, TR-RO also starts with the empty stage where no electron occupies the dot as shown in Fig. 7. Then both the energy level of the triplet and the singlet states are pulled below the reservoir and an electron with unknown spin tunnels in. After the wait time $t_{\rm wait}$ ($\Gamma_S^{-1} \gg t_{\rm wait} \gg \Gamma_T^{-1}$), the electron with the triplet state is much more likely to tunnel out. Then the spin state can be converted to a charge current and precisely detected. This method is effective even when the energy difference between two spin states is very small.

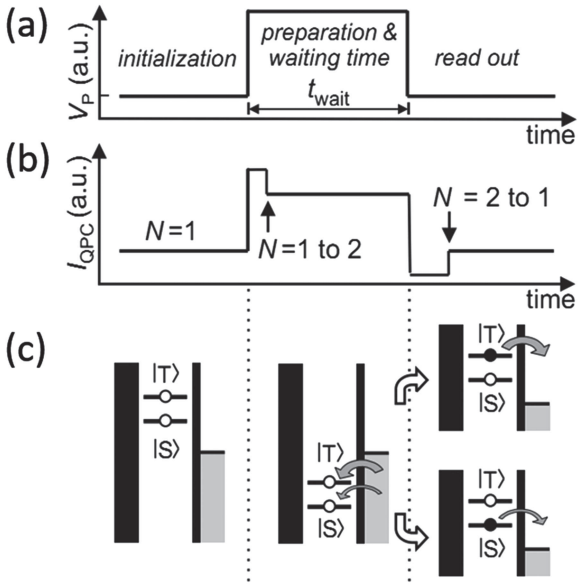


Fig. 7. (color online) Diagrams of single-shot readout with TR-RO. (a) Shape of gate pulses applied to the gate to control the measurement. (b) Response of QPC signals corresponding to the pulses. (c) Energy diagram of the three steps of the spin-to-charge conversion. The figure comes from Ref. [81].

5. Definition of spin qubits

A two-level system can be encoded as a qubit. We can describe a qubit on a Bloch sphere. In Fig. 8, the north pole of the sphere represents $|0\rangle$ and the south pole represents $|1\rangle$. Every point on this sphere represents an arbitrary state $|\psi\rangle = \alpha|0\rangle + \beta|1\rangle$, with two complex number α and β satisfying $|\alpha|^2 + |\beta|^2 = 1$. On the Bloch sphere, the polar angle θ represents the probability coefficient of the state, while the azimuthal angle φ is the phase of the qubit.

$$\varphi = \sin\theta\cos\varphi\boldsymbol{x} + \sin\theta\sin\varphi\boldsymbol{y} + \cos\theta\boldsymbol{z}, \tag{1}$$

where $\boldsymbol{x}$, $\boldsymbol{y}$, and $\boldsymbol{z}$ are the unit vectors of the coordinate axis.

In quantum dot systems, one can encode qubits on both the charge states and the spin states. However, noise disturbance severely limits the coherence of charge states, compared to spin states. There are several types of spin qubits determined by different encoding methods. Loss–DiVincenzo qubits (LD qubits)[10–12,17,84] and singlet-triplet qubits (ST qubits)[8,9] are primarily investigated. Usually, the basis states for a LD qubit are two independent spin states without entanglement, while that for ST qubits are the superposition of states defined as $|S\rangle = (|\uparrow\downarrow\rangle - |\downarrow\uparrow\rangle)/\sqrt{2}$ and $|T_0\rangle = (|\uparrow\downarrow\rangle + |\downarrow\uparrow\rangle)/\sqrt{2}$ states. Most established researchers in the field of quantum dots are focused on these two types. Besides, exchange-only qubits,[85] resonant-exchange qubits,[86] and hybrid qubits[87–90] are also investigated due to their individual advantages. For example, a hybrid qubit could speed up the implementation of gate operations and maintain a longer coherence time.[91]

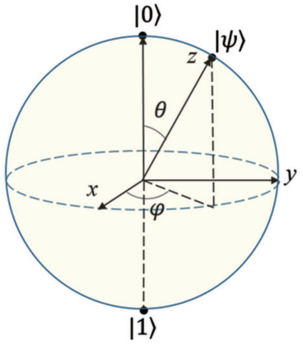


Fig. 8. (color online) Bloch sphere corresponding to the state of an electron spin qubit. Any state $|\psi\rangle$ is a superposition state of $|0\rangle$ and $|1\rangle$ represented as $|\psi\rangle = \cos(\theta/2)|0\rangle + e^{i\varphi}\sin(\theta/2)|1\rangle$.

6. Spin interaction with the environment

6.1. Spin–orbit interaction

In quantum dot systems, the spin states are affected by the environment.[92] Spin–orbit interaction is one of the dominant factors. Usually, this effect is treated as a small perturbation as long as the size of the dot is much smaller than the spin–orbit length $l_{\rm SO}$. In the case of GaAs (zinc-blend structure), it is suitable to focus on the linear part of the D'yakonov–Perel mechanism[93] although a spin may flip via the Elliot–Yafet mechanism[94] or the Bir–Aronov–Pikus mechanism.[95] The linear Hamiltonian is given by

$$H_{\rm SO} = \alpha(p_x\sigma_y - p_y\sigma_x) + \beta(p_x\sigma_x + p_y\sigma_y), \tag{2}$$

which is the sum of the Rashba (α) and Dresselhaus (β) spin–orbit interactions. Both of them mix up the spin and orbit states.[96] For a double quantum dot, singlet and triplet states are also affected because they are involved with the orbital states.

6.2. Hyperfine interaction

Nuclear-spin induced hyperfine interaction results in some consequences.[6] Leakage current of the Pauli spin blockade regime is one of these consequences which has been experimentally demonstrated.[97,98] Besides, it has been proved that the electron spin could be flipped via hyperfine interaction.[8]

7. Manipulation of electron spin

7.1. Single spin operation

As previously indicated, the spin states can be represented by any point on the Bloch sphere, and $|\psi\rangle = \alpha|0\rangle + \beta|1\rangle$ could be written as $|\psi\rangle = \cos(\theta/2)|0\rangle + e^{i\phi}\sin(\theta/2)|1\rangle$, where θ is the probability coefficient of the state and ϕ is the phase of the qubit. The spin state could evolve to another arbitrary state after a unitary operation U, which can be recognized as an Euler rotation. Any Euler rotation around x, y, or z is written as $R(\theta) = \exp(-i\theta\sigma/2)$, where σ is any one of the Pauli spin matrices and θ is the angle of rotation. For example, $X = \exp(-i\pi\sigma_x/2)$ is the rotation around x, analogous to the classical NOT gate from $|0\rangle$ to $|1\rangle$. Similarly, Z is the rotation of a spin state around the z-axis and is related to the behavior of an electron spin under a static magnetic field. The system is described by the Hamiltonian $H = E_z\sigma_z/2$, $E_z = \hbar\omega_z$ is the Zeeman energy. This implies that the static magnetic field (B_z) drives an electron spin rotating around the z-axis at the Larmor frequency ω_z. A rotation around the x-axis (or an axis in the x–y plane) and another rotation around the z-axis make up the universal single spin operation.

There are several methods for achieving this spin operation, which are divided into two categories. They are electron spin resonance (ESR) and electric dipole spin resonance (EDSR), and they follow different mechanisms. For ESR, spin operations are achieved by controlling an alternating magnetic field while the EDSR is manipulated completely by electrical means. Several experiments will be discussed in detail to clarify the spin resonance dynamics.

7.1.1. Electron spin resonance

Driven coherent rotation of a single spin has been realized in several solid systems using electron spin resonance (ESR).[99–101] It was proposed by Engel and Loss in a single quantum dot,[102,103] but was realized in GaAs double quantum dots. The first ESR experiment in quantum dots was demonstrated by Koppens *et al.*[84] Later, it was also demonstrated in a single dot in Si-MOS.[11] In the ESR technique, an oscillating magnetic field $\boldsymbol{B}_{AC}$ with an angular frequency ω along the x-axis and a static magnetic field B_z are applied along the z-axis. $\boldsymbol{B}_{AC}$ is used to achieve spin-flip while B_z induces the Zeeman energy $E_z = g\mu_B B_z$ where μ_B is the Bohr magneton and g is the electron g-factor. The rotation induced by B_z is described as the motion in a coordinate system rotating around the z-axis with rotating frequency $\omega_z = g\mu_B B_z/\hbar$, and the spin state becomes $|\psi\rangle^{rot} = \exp(i\omega_z t\sigma_z/2)|\psi\rangle$. Assuming $\boldsymbol{B}_{AC} = \boldsymbol{x}B_{AC}\cos(\omega t + \varphi)$, we can obtain the Hamiltonian

$$H = \frac{\mu_B g B_z}{2}\sigma_z + \frac{\mu_B g B_{AC}}{2}\sigma_x\cos(\omega t + \varphi). \tag{3}$$

When the Hamiltonian is reduced in the rotating frame followed by the rotating wave approximation, we have

$$H_R = \frac{\hbar(\omega_z - \omega)}{2}\sigma_z + \frac{\hbar\omega_1}{2}[\sigma_x\cos\varphi - \sigma_y\sin\varphi], \tag{4}$$

where $\omega_1 = \mu_B g B_{AC}/(2\hbar)$. The rotation of the spin state is controlled by ω_z and ω around the z-axis. When the ac field angular frequency $\omega = \omega_z$, there will be only rotation around a fixed axis in the x–y plane controlled by ω_1, which is known as the Rabi oscillation. To simplify the situation, we usually adjust $\varphi = 0$ and the spin state rotates between $|0\rangle$ and $|1\rangle$ around the x-axis. Therefore, the Rabi oscillation realizes a NOT gate when a π pulse is applied such that the length of the pulse is $T\pi = \pi/\omega_1$. In addition, if the frequency ω does not match ωz, the spin will precess around the angle $\vartheta = \arctan[(\omega_z - \omega)/\omega_1]$ with frequency $\omega_2 = \sqrt{\omega_1^2 + (\omega_z - \omega)^2}$. By changing the magnetic field pulses, it is possible to arbitrarily control the qubit.

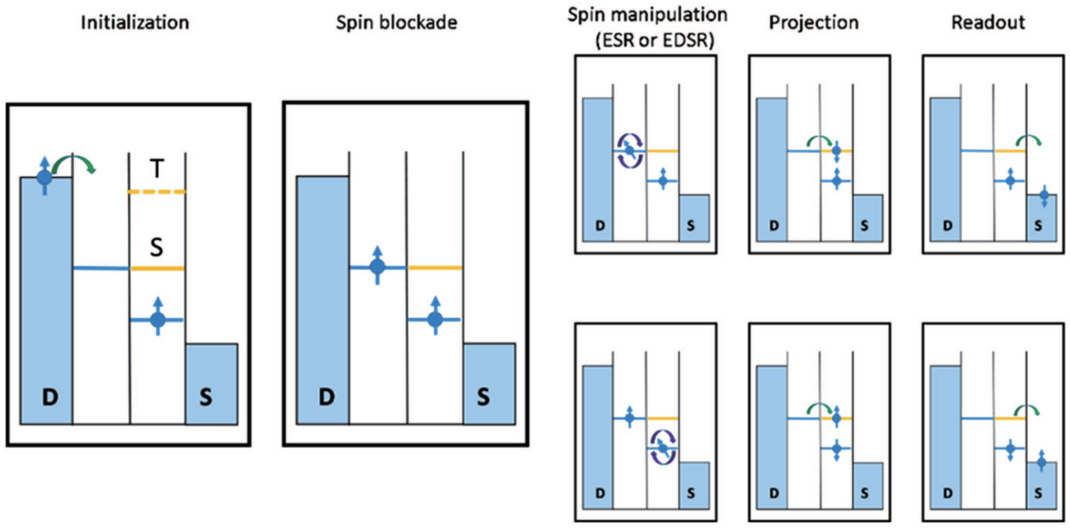


Fig. 9. (color online) Schematic diagram of the energy level during the ESR or EDSR measurement. It consists of initialization, spin blockade, spin manipulation, projection, and readout. Spin-flip is achieved in the spin manipulation step by hyperfine interaction,[8,104] spin–orbit interaction,[105] inhomogeneous magnetic field,[106] and g-factor tensor modulation.[107]

In the experiment, double quantum dots are tuned to a spin blockade regime where each dot is occupied by one electron. Due to the Zeeman energy, triplet states split into T_0, T_-, and T_+ states. Considering the lowest two energy states, the S and T_+ as shown in Fig. 9, the $T_+(1,1)$ state blocks the current as soon as the double dot is occupied by two parallel spins (one electron in each dot). To lift the blockade and generate current, the spin in the left (right) should be flipped. Both ESR and EDSR are able to achieve this requirement. In Koppens' experiment,[84] the alternating magnetic field $B_{\rm AC}$ works as an element of the spin-flip. During manipulation, a RF burst (blue line in Fig. 10(a)) is used to generate the ac magnetic field which can flip the spin states. Throughout the transport measurement in Fig. 10(b), there is a clear ESR response when sweeping the static magnetic field and the RF frequency. Two oblique lines represent the resonant frequencies dependence on the magnetic field. In a state of resonance, the spin state could change from up to down. Thus the electron can tunnel out of the dot. This could only happen when one of the electron spin rotates over $(2n+1)\pi$. The oblique lines are the characteristic signatures of the ESR, and the slope of the line can be used to fit the g-factor of the system.

In Fig. 10(c), the measured peak current oscillates periodically with a RF burst length which verifies the Rabi oscillation, which can be used to fit the coherence time T_2^*. In the inset of Fig. 10(d), the Rabi oscillation frequency linearly depends on the RF burst amplitude. In this system, the coherence time T_2^* was 10–20 ns and the fidelity reached 73%. In order to create the ac magnetic field, the coils are conductive with a current of approximately 1 mA. In this situation, the high heating power and large-area coils limit potential future applications and integrations.

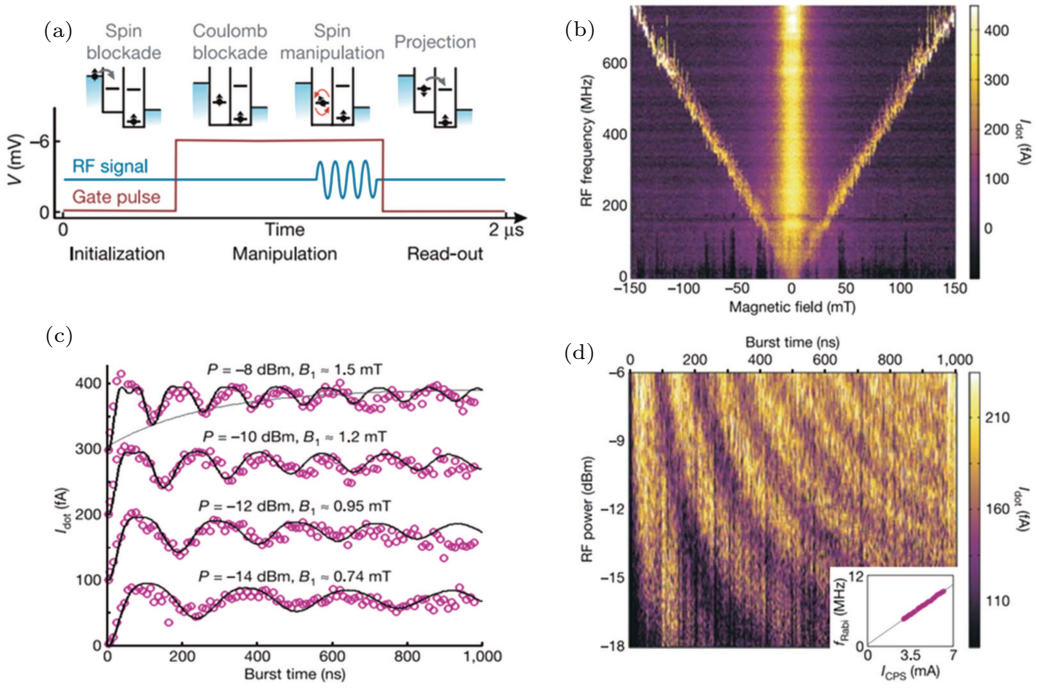


Fig. 10. (color online) (a) Sequences of pulse and microwaves used to control electron spin. (b) Measured transport current of the dots by sweeping the static magnetic field and RF burst frequency. (c) Coherent single spin rotation as a function of the RF burst time. (d) Rabi oscillation of the ESR experiment. The inset of (d) shows evidence of Rabi frequency dependence on RF power. The figure comes from Ref. [84].

7.1.2. Electric dipole spin resonance

To overcome the disadvantages of ESR, electric dipole spin resonance (EDSR) was theoretically proposed with a spin–orbit interaction (SOI)[108] and an inhomogeneous magnetic field,[109] as the medium to couple the electric field to the electron spin while an ac magnetic field couples to the spin states directly for ESR. In addition, hyperfine interaction[104] and g-tensor modulation resonance (g-TMR)[110] could be the mediating mechanism in the experiment.

Spin–orbit interaction In an EDSR setup, a static magnetic field $\boldsymbol{B}_z$ is applied to the device and an ac driving electric field $\boldsymbol{E}(t)$ is introduced to control spin. In contrast to ESR, EDSR couples orbital states to spin states when SOI works as a mediator. The effective Hamiltonian is given by[108]

$$H = H_{\rm Dot} + H_Z + H_{\rm SOI}, \tag{5}$$

$$H_Z = \frac{1}{2} g\mu \boldsymbol{B}_z \cdot \boldsymbol{\sigma}, \tag{6}$$

$$H_{\rm SOI} = \frac{1}{2} g\mu \boldsymbol{B}_{\rm eff} \cdot \boldsymbol{\sigma}, \tag{7}$$

where $\boldsymbol{B}_{\rm eff}$ is the effective SOI driving field caused by the electric field. Assuming the static external $\boldsymbol{B}_z$ and electric field $\boldsymbol{E}(t)$ are along [110] or [1$\bar{1}$0], then the value of $\boldsymbol{B}_{\rm eff}$ can be

written as

$$|\boldsymbol{B}_{\rm eff}| = 2|\boldsymbol{B}_{\rm z}|\frac{eE(t)l_{\rm dot}^2}{l_{\rm so}\cdot\Delta}, \tag{8}$$

where the spin–orbit length is defined as $l_{\rm so} = \hbar/m^*(\alpha+\beta)$, $l_{\rm dot}$ is the size of the dot, Δ is the orbital energy splitting, m^* is the effective mass, $\hbar$ is the reduced Planck constant, and α and β are the Rashba and Dresselhaus spin–orbit coefficients. As a consequence, $\boldsymbol{E}(t)$ could drive the spin rotating along the x-axis through $H_{\rm SOI}$. The speed of manipulation depends on Δ. In essence, it can be seen as the shift of center of the electron wave function in the dot caused by an electric field. Shifting $\Delta x = (eE(t)l_{\rm dot}^2)/\Delta$, we can obtain

$$|\boldsymbol{B}_{\rm eff}| = 2|\boldsymbol{B}_{z}|\frac{\Delta x}{l_{\rm so}}, \tag{9}$$

In the first EDSR experiment,[105] an ac electric field $\boldsymbol{E}(t)$ and $\boldsymbol{B}_z$ are along the [110] direction where the SOI is much more pronounced than the other directions. As shown in Fig. 11(c), oscillations are observed. The frequency of the oscillation increases linearly as a function of the amplitude of the microwave. It is the signature of the Rabi oscillation between spin states, which confirms EDSR. It is worth mentioning that with a certain device design, SOI is suppressed. Under this circumstance, hyperfine interaction dominates the experiment, resulting in the absence of Rabi oscillations.[104]

Inhomogeneous magnetic field We can assume that the static magnetic field B_0 is applied in the x-direction, and the inhomogeneous field is given by

$$\boldsymbol{B}_{\rm sl}(x) = b_{\rm sl}x\boldsymbol{z}, \tag{10}$$

where $b_{\rm sl}$ is the slanting magnetic field gradient in the x-direction. As previously indicated, the ac electric field causes a shift of the center of the electron wave function: $\Delta x = (eE(t)l_{\rm dot}^2)/\Delta$, leading to an effective alternating magnetic field $\boldsymbol{B}_{\rm eff}$,

$$\boldsymbol{B}_{\rm eff}(t) = -b_{\rm sl}\cdot\frac{eE(t)l_{\rm dot}^2}{\Delta}\boldsymbol{z}. \tag{11}$$

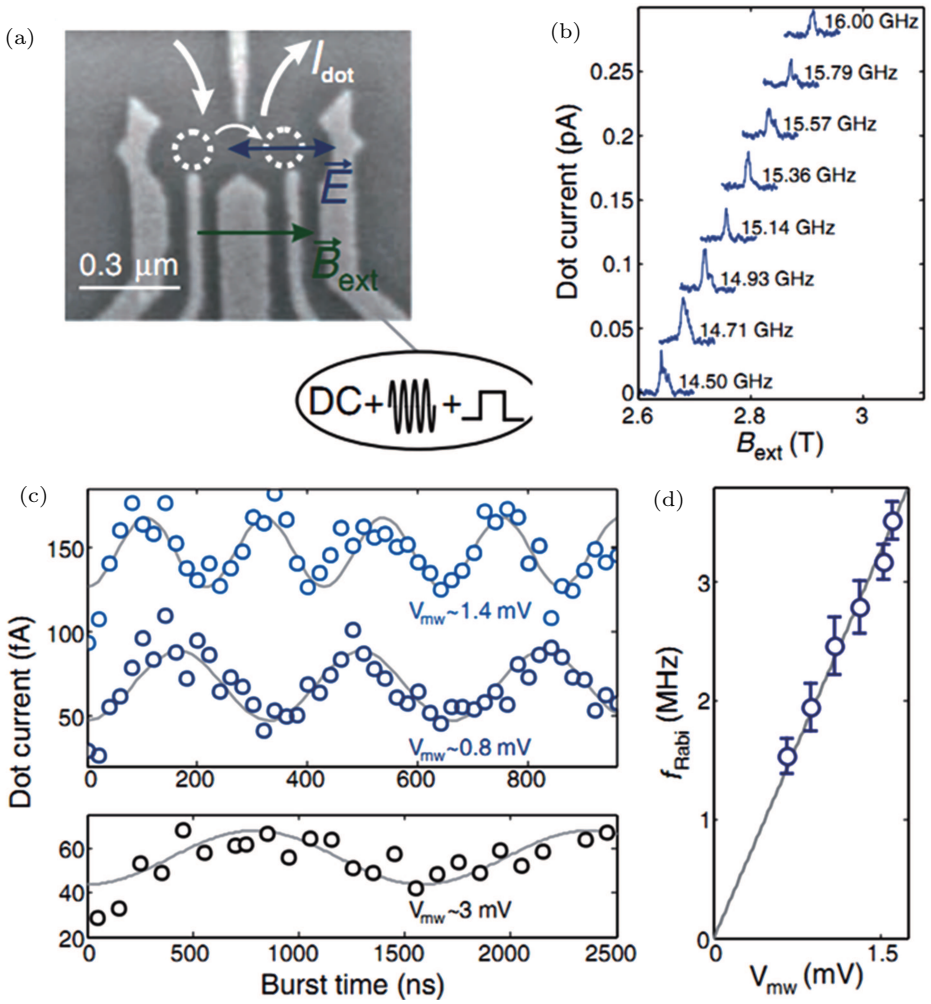


Fig. 11. (color online) (a) Scanning electron micrograph of the GaAs double quantum dots. The blue arrow indicates the electric field and the green arrow is the direction of the static magnetic field. (b) Resonance of spin-flip by changing the amplitude of the magnetic field and the RF frequency. (c) Rabi oscillation of the EDSR experiment. The period changes along with the amplitude of the microwave. (d) Rabi frequency as a function of amplitude of the microwave (the square root of MW power). The figure comes from Ref. [105].

Figure 12(a) shows the on-chip micro-magnet device. The yellow part is the micro-magnet made of cobalt, on top of GaAs double quantum dots. In Fig. 12(b), an illustration of the schematic diagram of the micro-magnet is presented as it creates the slanting field, as long as the magnet is in a magnetic field. In Figs. 12(c) and 12(d), the resonances of the electron spins in both dots are detected simultaneously. If the micro-magnet is properly designed, a large Zeeman splitting is achieved to individually manipulate each electron spin.[10,17]

Tensor modulation resonance (g-TMR) In the experiment, the g-factor is designed to be anisotropic and depends on the voltage so that it is treated as a gate-dependent tensor. Then the Hamiltonian is

$$H_Z = \frac{1}{2} g\mu \boldsymbol{B}_0 \cdot \boldsymbol{\sigma} = \boldsymbol{S} \cdot \boldsymbol{\Omega}, \tag{12}$$

where $\boldsymbol{B}_0$ is the magnetic field with angle θ from the z-axis. $\boldsymbol{S} = \frac{\hbar}{2}\boldsymbol{\sigma}$ are the Pauli spin matrices and $\boldsymbol{\Omega}$ is the precession vector. Since the g-tensor is designed to be dependent on the position z in the growth direction, then the vector is expanded along the z-axis

$$\boldsymbol{\Omega}(z) = \boldsymbol{\Omega}_0 + \boldsymbol{\Omega}\|(z) + \boldsymbol{\Omega}_\perp(z), \tag{13}$$

where $\boldsymbol{\Omega}_0$ is the offset and time-independent term, $\boldsymbol{\Omega}\|$ and $\boldsymbol{\Omega}_\perp$ are the parallel and perpendicular parts of the first Taylor series of the precession axis vector around $z = 0$, which is stable for electron. The components $\boldsymbol{\Omega}\|$ and $\boldsymbol{\Omega}_\perp$ correspond to the rotating frequency $\omega_\|$ and $\omega_\perp$, respectively. The frequency $\omega_\perp$ flips the spin state

$$\omega_\perp = \frac{\mu_B}{\hbar} B_0 \frac{\partial(g_\pi - g_0)}{\partial z} \sin\theta\cos\theta \begin{pmatrix} \cos\theta \\ 0 \\ -\sin\theta \end{pmatrix}, \tag{14}$$

where g_π and g_0 are the in-plane and out-plane parts of the g-tensor. The first electric controlled g-TMR experiment was demonstrated in 2001.[111] Later, Gigahertz electron spin manipulation was achieved.[107] To date, no Rabi oscillations are realized by this approach.

All the previously discussed were firstly demonstrated in GaAs systems. By employing the same mechanisms, similar experiments were also performed in other systems, such as Si-MOS,[13] Si/SiGe quantum well,[14,16] and so on.

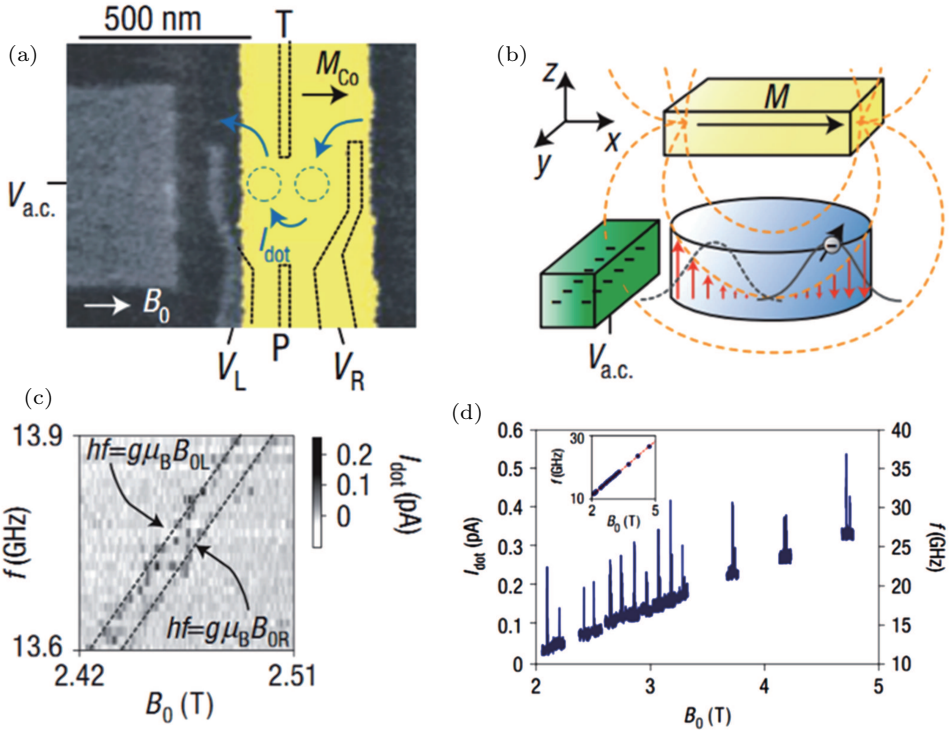


Fig. 12. (color online) (a) Scanning electron micrograph of the device made on a GaAs heterostructure. The yellow part is the cobalt micro-magnet used to generate a slanting magnetic field. (b) The schematic diagram of the magnetic field generated by the colt magnets. (c) Typical EDSR lines indicating the spin-flip mechanism. Two lines correspond to behaviors in the left dot and the right dot. (d) Position of both resonance peaks in two dots by sweeping the magnetic field. The figure comes from Ref. [106].

7.2. Two-spin operations

CNOT, C-phase (control-phase), and swap operation are basic two-qubit operations which are essential for universal control of qubits.[108] The CNOT gate with relative high fidelities are achieved with Si-MOS and SiGe double quantum dots.[12,18] One of the experiments is discussed here to clarify the details.

In the experiment,[17] a DQD is formed on a SiGe heterostructure with an on-chip micro-magnet. As shown in Figs. 13(a) and 13(b), gates L and R are used to confine the

dots. By sweeping the gate voltage, the few-electron regime can be obtained with charge sensing. The manipulation works at the point marked as 'd' in Fig. 13(b), with only one electron in each quantum dot. High-fidelity single qubit control is demonstrated when the frequency of the microwave matches the resonance frequency of the spin in the left (right) dot, as shown in Fig. 13(c).

Considering two-spin operations, the time-dependent Hamiltonian can be written as[113]

$$H = J(t)\left(\boldsymbol{S}_{\rm L}\cdot\boldsymbol{S}_{\rm R} - \frac{1}{4}\right) + \boldsymbol{B}_{\rm L}\cdot\boldsymbol{S}_{\rm L} + \boldsymbol{B}_{\rm R}\cdot\boldsymbol{S}_{\rm R}, \quad (15)$$

where J is the time-dependent exchange coupling between two spins. $\boldsymbol{S}_{\rm L}(\boldsymbol{S}_{\rm R})$ is the electron spin in the left (right) dot. Then the eigenvalues are written as

$$\varepsilon(|\uparrow\uparrow\rangle) = E_z + (B^{m,1}_{z,\rm L} + B^{m,1}_{z,\rm R})/2, \quad (16)$$

$$\varepsilon(|\tilde{\uparrow\downarrow}\rangle) = \left(-J - \sqrt{J^2 + \left(\delta E - \left(B^{m,1}_{z,\rm L} - B^{m,1}_{z,\rm R}\right)\right)^2}\right)/2, \quad (17)$$

$$\varepsilon(|\tilde{\downarrow\uparrow}\rangle) = \left(-J + \sqrt{J^2 + \left(\delta E - \left(B^{m,1}_{z,\rm L} - B^{m,1}_{z,\rm R}\right)\right)^2}\right)/2, \quad (18)$$

$$\varepsilon(|\downarrow\downarrow\rangle) = -E_z - (B^{m,1}_{z,\rm L} + B^{m,1}_{z,\rm R})/2, \quad (19)$$

where $E_z = (B^{\rm ext}_z + B^{m,0}_{z,\rm L} + B^{\rm ext}_z + B^{m,0}_{z,\rm R})/2$ and $\delta E_z = (B^{\rm ext}_z + B^{m,0}_{z,\rm R} - B^{\rm ext}_z - B^{m,0}_{z,\rm L})$. $B^{\rm ext}_z$ is the static magnetic field, and the on-chip micro-magnet creates $B^{m}_{z,\rm L(R)}(t) = B^{m,0}_{z,\rm L(R)} + B^{m,1}_{z,\rm L(R)}(t)$ which consists of a static part and a time-dependent part. The tilde represents the hybridization of $|\downarrow\uparrow\rangle$ and $|\uparrow\downarrow\rangle$.

Given the eigenvalues of the Hamiltonian, it is reasonable to define the corresponding transition frequencies as

$$f^{\rm L}_{|\psi_{\rm R}\rangle=|\downarrow\rangle} = |\varepsilon(|\downarrow\downarrow\rangle) - \varepsilon(|\tilde{\uparrow\downarrow}\rangle)|, \quad (20)$$

$$f^{\rm L}_{|\psi_{\rm R}\rangle=|\uparrow\rangle} = |\varepsilon(|\tilde{\downarrow\uparrow}\rangle) - \varepsilon(|\uparrow\uparrow\rangle)|, \quad (21)$$

$$f^{\rm R}_{|\psi_{\rm L}\rangle=|\downarrow\rangle} = |\varepsilon(|\downarrow\downarrow\rangle) - \varepsilon(|\tilde{\downarrow\uparrow}\rangle)|, \quad (22)$$

$$f^{\rm R}_{|\psi_{\rm L}\rangle=|\uparrow\rangle} = |\varepsilon(|\tilde{\uparrow\downarrow}\rangle) - \varepsilon(|\uparrow\uparrow\rangle)|. \quad (23)$$

Figure 14(b) plots the eigenvalues (16)–(19) as a function of the exchange coupling J and marks the transitions. In Fig. 13(d), it is obvious that two resonances occur ($f^{\rm L}_{|\psi_{\rm R}\rangle=|\downarrow\rangle}$ and $f^{\rm L}_{|\psi_{\rm R}\rangle=|\uparrow\rangle}$) when sweeping with probe frequency $f_{\rm p}$. Rabi oscillations of the left spin depend on the state of the right spin. This is because the state of the right spin affects the frequency of transition shown in Fig. 14(b).

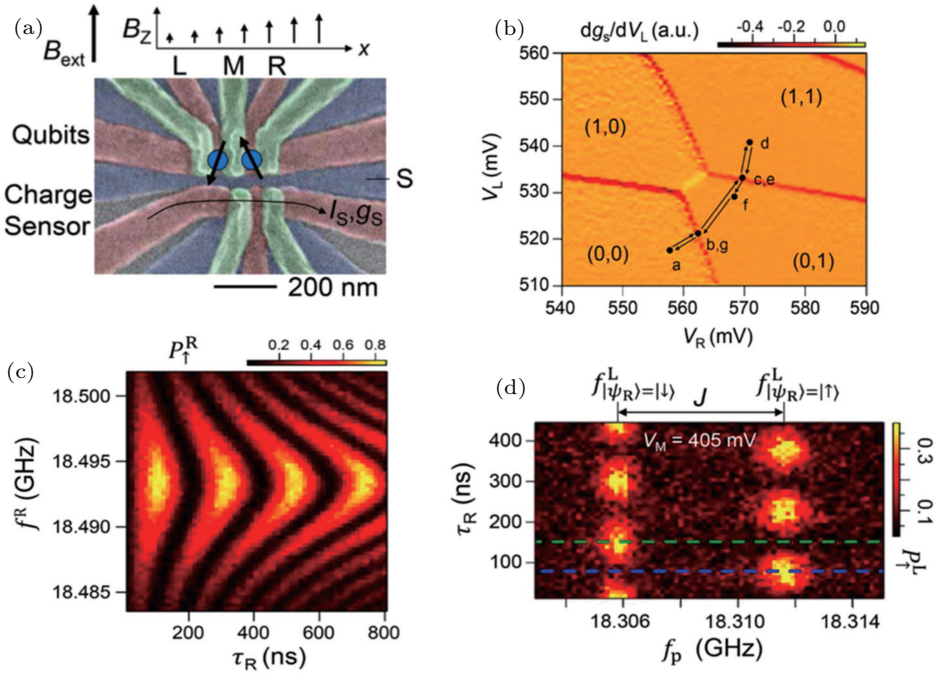


Fig. 13. (color online) (a) Scanning electron micrograph of the SiGe double quantum dots. (b) Stability diagram of the DQD and schematic of different steps during operations (marked by black points). (c) Rabi oscillations between spin-up and spin-down state of the electron in the right dot. (d) $P^{\rm L}_{\uparrow}$ as a function of $\tau_{\rm R}$ and probe frequency $f_{\rm p}$. There are two resonances of the left qubit and their frequencies are split by J. The response of the left spin qubit oscillates between these two frequencies as the right qubit oscillates between spin-up and spin-down. The figure comes from Ref. [17].

The CNOT gate is achieved by tuning J and the frequency of the microwave. Using appropriate gate pulses, J can be tuned in a suitable range leading to the difference of the transition frequencies ($f^{\rm L}_{|\psi_{\rm R}\rangle=|\uparrow\rangle}$ and $f^{\rm L}_{|\psi_{\rm R}\rangle=|\downarrow\rangle}$). In CNOT gate operation, it is assumed that the left spin is the target qubit and the right spin is the control qubit. Microwaves with frequency ($f^{\rm L}_{|\psi_{\rm R}\rangle=|\uparrow\rangle}$) that match the energy difference between $|\uparrow\uparrow\rangle$ and $|\tilde{\downarrow\uparrow}\rangle$ are applied. Figure 14(a) plots the spin-up probability of both electrons ($P^{\rm L}_{\uparrow}$ and $P^{\rm R}_{\uparrow}$) as a function of the microwave duration $\tau_{\rm P}$. When the control qubit is initialized to the spin-up (spin-down) state, the left spin can (cannot) rotate between up and down, as illustrated. This implies that a flip of the target

qubit occurs only when the control qubit is initialized to the up-state. The dashed vertical line which indicates the pulse sequence with $\tau_P = 130$ ns represents the CNOT gate. Finally, the CNOT gate must be able to operate on an arbitrary initial state. In Fig. 14(c), the spin-up probability of both electrons ($P_\uparrow^L$ and $P_\uparrow^R$) are plotted at the working point indicated by the dashed line in Fig. 14(a). The dependence between $P_\uparrow^L$ and $P_\uparrow^R$ is an indication of a CNOT operation with an arbitrary initial state.

Other spin operations, such as x rotation based on two electron spins[10] and a two-qubit operation using two ST qubits in GaAs quantum dots have also been demonstrated.[9] In addition, two-spin qubits in GaAs quantum dot operations in other systems have also been performed. Recently, two-qubits operation in Si-MOS[12] and Si/SiGe[18] systems were demonstrated. Future experiments may focus on inhomogeneous magnetic field to achieve spin manipulation.

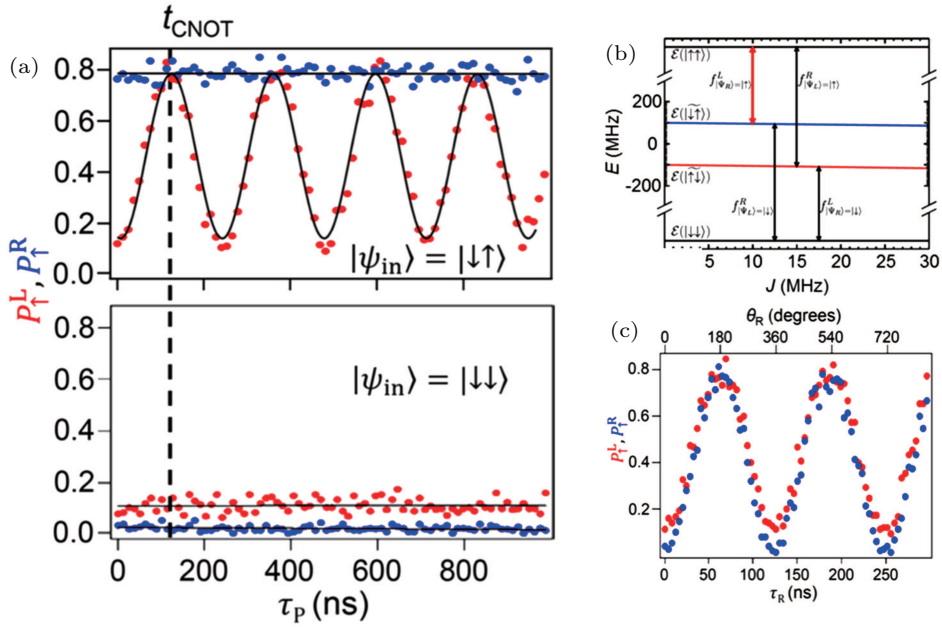


Fig. 14. (color online) (a) $P_\uparrow^L$ and $P_\uparrow^R$ as a function of τ_P for different input states $|\psi_{in}\rangle$. The CNOT gate operation indicated by the dash line. (b) Eigenvalues as a function of exchange coupling J. (c) CNOT gate with superposition input states. The response shows that the target qubit follows the state of the control qubit. The figure comes from Ref. [17].

8. Outlook

Over the past few years, multiple qubits have been demonstrated in quantum dot systems. Further breakthroughs are needed to achieve entanglement of different states, quantum error correction, and so on. The fidelity of qubits is one of their key features, and the highest reported level approaches 90% of the Bell states[18] and 99% of a single-qubit gate.[12,17] In order to realize reliable quantum information processing using quantum dot systems, it is necessary to improve their fidelity and scalability in the next few years.

References

[1] Reed M A, Randall J N, Aggarwal R J, Matyi R J, Moore T M and Wetsel A E 1988 *Phys. Rev. Lett.* **60** 535

[2] Ashoori R C, Stormer H L, Weiner J S, Pfeiffer L N, Baldwin K W and West K W 1993 *Phys. Rev. Lett.* **71** 613

[3] Kastner M A 1993 *Phys. Today* **46** 1

[4] Tarucha S, Austing D G, Honda T, van der Hage R J and Kouwenhoven L P 1996 *Phys. Rev. Lett.* **77** 3613

[5] Loss D and DiVincenzo D P 1998 *Phys. Rev. A* **57** 120

[6] Ono K, Austing D G, Tokura Y and Tarucha S 2002 *Science* **297** 1313

[7] Elzerman J M, Hanson R, van Beveren L H W, Witkamp B, Vandersypen L M K and Kouwenhoven L P 2004 *Nature* **430** 431

[8] Petta J R, Johnson A C, Taylor J M, Laird E A, Yacoby A, Lukin M D, Marcus C M, Hanson M P and Gossard A C 2005 *Science* **309** 2180

[9] Shulman M D, Dial O E, Harvey S P, Bluhm H, Umansky V and Yacoby A 2012 *Science* **336** 202

[10] Brunner R, Shin Y S, Obata T, Pioro-Ladriere M, Kubo T, Yoshida K, Taniyama T, Tokura Y and Tarucha S 2011 *Phys. Rev. Lett.* **107** 146801

[11] Pla J J, Tan K Y, Dehollain J P, Lim W H, Morton J J, Jamieson D N, Dzurak A S and Morello A 2012 *Nature* **489** 541

[12] Veldhorst M, Yang C H, Hwang J C, Huang W, Dehollain J P, Muhonen J T, Simmons S, Laucht A, Hudson F E, Itoh K M, Morello A and Dzurak A S 2015 *Nature* **526** 410

[13] Maur R, Jehl X, Kotekar-Patil D, Corna A, Bohuslavskyi H, Lavieville R, Hutin L, Barraud S, Vinet M, Sanquer M and De Franceschi S 2016 *Nat. Commun.* **7** 13575

[14] Maune B M, Borselli M G, Huang B, Ladd T D, Deelman P W, Holabird K S, Kiselev A A, Alvarado-Rodriguez I, Ross R S, Schmitz A E, Sokolich M, Watson C A, Gyure M F and Hunter A T 2012 *Nature* **481** 344

[15] Kawakami E, Scarlino P, Ward D R, Braakman F R, Savage D E, Lagally M G, Friesen M, Coppersmith S N, Eriksson M A and Vandersypen L M 2014 *Nat. Nanotechnol.* **9** 666

[16] Wu X, Ward D R, Prance J R, Kim D, Gamble J K, Mohr R T, Shi Z, Savage D E, Lagally M G, Friesen M, Coppersmith S N and Eriksson M A 2014 *Proc. Natl. Acad. Sci.* **111** 11938

[17] Zajac D M, Sigillito A J, Russ M, Borjans F, Taylor J M, Burkard G and Petta J R 2017 *Science* **359** 439

[18] Watson T F, Philips S G J, Kawakami E, Ward D R, Scarlino P, Veldhorst M, Savage D E, Lagally M G, Friesen M, Coppersmith S N, Eriksson M A and Vandersypen L M K 2018 *Nature* **555** 633

[19] Ashoori R C 1996 *Nature* **379** 413
[20] Fitzgerald E A 1992 *J. Vac. Sci. & Technol. B: Microelectronics Nanometer Struct.* **10** 1807
[21] Monroe D, Xie Y H, Fitzgerald E A and Silverman P J 1992 *Phys. Rev. B* **46** 7935
[22] Ismail K, Arafa M, Saenger K L, Chu J O and Meyerson B S 1995 *Appl. Phys. Lett.* **66** 1077
[23] Rokhinson L P, Guo L J, Chou S Y and Tsui D C 2001 *Phys. Rev. Lett.* **87** 116802
[24] Lu T M, Luhman D R, Lai K, Tsui D C, Pfeiffer L N and West K W 2007 *Appl. Phys. Lett.* **90** 112113
[25] Lu T M, Tsui D C, Lee C H and Liu C W 2009 *Appl. Phys. Lett.* **94** 182102
[26] Wang L J, Cao G, Tu T, Li H O, Zhou C, Hao X J, Guo G C and Guo G P 2011 *Chin. Phys. Lett.* **28** 67301
[27] Wang L J, Guo G P, Wei D, Cao G, Tu T, Xiao M, Guo G C and Chang A M 2011 *Appl. Phys. Lett.* **99** 112117
[28] Wang L J, Li H O, Tu T, Cao G, Zhou C, Hao X J, Su Z, Xiao M, Guo G C, Chang A M and Guo G P 2012 *Appl. Phys. Lett.* **100** 022106
[29] Luo G, Zhang Z Z, Deng G W, Li H O, Cao G, Xiao M, Guo G C and Guo G P 2017 *Nanoscale* **9** 5608
[30] Ponomarenko L A, Schedin F, Katsnelson M I, Yang R, Hill E W, Novoselov K S and Geim A K 2008 *Science* **320** 356
[31] Luo G, Zhang Z Z, Li H O, Song X X, Deng G W, Cao G, Xiao M and Guo G P 2017 *Front. Phys.* **12** 128502
[32] Zhang Z Z, Song X X, Luo G, Deng G W, Mosallanejad V, Taniguchi T, Watanabe K, Li H O, Cao G, Guo G C, Nori F and Guo G P 2017 *Sci. Adv.* **3** e1701699
[33] Song X X, Liu D, Mosallanejad V, You J, Han T Y, Chen D T, Li H O, Cao G, Xiao M, Guo G C and Guo G P 2015 *Nanoscale* **7** 16867
[34] Song X X, Zhang Z Z, You J, Liu D, Li H O, Cao G, Xiao M and Guo G P 2015 *Sci. Rep.* **5** 16113
[35] Wang K, Greve K De, Jauregui L A, Sushko A, High A, Zhou Y, Scuri G, Taniguchi T, Watanabe K, Lukin M D, Park H and Kim P 2018 *Nat. Nanotechnol.* **13** 128
[36] Laird E A, Kuemmeth F, Steele G A, Grove-Rasmussen K, Nygard J, Flensberg K and Kouwenhoven L P 2015 *Rev. Mod. Phys.* **87** 703
[37] Ismail K, Meyerson B S and Wang P J 1991 *Appl. Phys. Lett.* **58** 2117
[38] Notargiacomo A, Di L, Scappucci G, Mariottini G, Evangelisti F, Giovine E and Leoni R 2003 *Appl. Phys. Lett.* **83** 302
[39] Angus S J, Ferguson A J, Dzurak A S and Clark R G 2007 *Nano Lett.* **7** 2051
[40] Lu T M, Liu J, Kim J, Lai K, Tsui D C and Xie Y H 2007 *Appl. Phys. Lett.* **90** 182114
[41] Li H O, Cao G, Xiao M, You J, Wei D, Tu T, Guo G C, Jiang H W and Guo G P 2014 *J. Appl. Phys.* **116** 174504
[42] Taylor J M, Petta J R, Johnson A C, Yacoby A, Marcus C M and Lukin M D 2007 *Phys. Rev. B* **76** 035315
[43] Andreas B, Azuma Y, Bartl G, *et al.* 2011 *Phys. Rev. Lett.* **106** 030801
[44] See A M, Klochan O, Hamilton A R, Micolich A P, Aagesen M and Lindelof P E 2010 *Appl. Phys. Lett.* **96** 112104
[45] Xiao M, House M G and Jiang H W 2010 *Appl. Phys. Lett.* **97** 032103
[46] Wang K, Payette C, Dovzhenko Y, Deelman P W and Petta J R 2013 *Phys. Rev. Lett.* **111** 096801
[47] Zajac D M, Hazard T M, Mi X, Wang K and Petta J R 2015 *Appl. Phys. Lett.* **106** 223507
[48] van der Wiel W G, Franceschi S De, Elzerman J M, Fujisawa T, Tarucha S and Kouwenhoven L P 2002 *Rev. Mod. Phys.* **75** 1
[49] Scheffler M, Nadj-Perge S, Kouwenhoven L P, Borgstrom M T and Bakkers E P A M 2008 *Physica E* **40** 1202
[50] Nadj-Perge S, Frolov S M, van Tilburg J W W, Danon J, Nazarov Y V, Algra R, Bakkers E P A M and Kouwenhoven L P 2010 *Phys. Rev. B* **81** 201305
[51] Brauns M, Ridderbos J, Li A, Bakkers E P A M, van der Wiel W G and Zwanenburg F A 2016 *Phys. Rev. B* **94** 041411
[52] Li S X, Li Y, Gao F, Xu G, Li H O, Cao G, Xiao M, Wang T, Zhang J J and Guo G P 2017 *Appl. Phys. Lett.* **110** 133105
[53] Elzerman J M, Hanson R, Greidanus J S, Willems van Beveren L H, De Franceschi S, Vandersypen L M K, Tarucha S and Kouwenhoven L P 2003 *Phys. Rev. B* **67** 161308
[54] Field M, Smith C G, Pepper M, Ritchie D A, Frost J E, Jones G A and Hasko D G 1993 *Phys. Rev. Lett.* **70** 1311
[55] Sprinzak D, Ji Y, Heiblum M, Mahalu D and Shtrikman H 2002 *Phys. Rev. Lett.* **88** 176805
[56] DiCarlo L, Lynch H J, Johnson A C, Childress L I, Crockett K, Marcus C M, Hanson M P and Gossard A C 2004 *Phys. Rev. Lett.* **92** 226801
[57] Wang K, Payette C, Dovzhenko Y, Deelman P W and Petta J R 2013 *Phys. Rev. Lett.* **111** 046801
[58] Shang R N, Li H O, Cao G, Xiao M, Tu T, Jiang H W, Guo G C and Guo G P 2013 *Appl. Phys. Lett.* **103** 162109
[59] Johnson A C, Petta J R, Marcus C M, Hanson M P and Gossard A C 2005 *Phys. Rev. B* **72** 165308
[60] Petta J R, Johnson A C, Marcus C M, Hanson M P and Gossard A C 2004 *Phys. Rev. Lett.* **93** 186802
[61] Elzerman J M, Hanson R, Willems van Beveren L H, Vandersypen L M K and Kouwenhoven L P 2004 *Appl. Phys. Lett.* **84** 4617
[62] Yang C H, Rossi A, Ruskov R, Lai N S, Mohiyaddin F A, Lee S, Tahan C, Klimeck G, Morello A and Dzurak A S 2013 *Nat. Commun.* **4** 2069
[63] Rossler C, Krahenmann T, Baer S, Ihn T, Ensslin K, Reichl C and Wegscheider W 2013 *New J. Phys.* **15** 033011
[64] Schoelkopf R J, Wahlgren P, Kozhevnikov A A, Delsing P and Prober D E 1998 *Science* **280** 1238
[65] Biercuk M J, Reilly D J, Buehler T M, Chan V C, Chow J M, Clark R G and Marcus C M 2006 *Phys. Rev. B* **73** 201402
[66] Sahoo S, Kontos T, Furer J, Hoffmann C, Gräber M, Cottet A and Schönenberger C 2005 *Nat. Phys.* **1** 99
[67] Jørgensen I H, Grove-Rasmussen K, Wang K Y, Blackburn A M, Flensberg K, Lindelof P E and Williams D A 2008 *Nat. Phys.* **4** 536
[68] Wang K Y, Blackburn A M, Wang H F, Wunderlich J and Williams D A 2013 *Appl. Phys. Lett.* **102** 093508
[69] Tsukagoshi K, Alphenaar B W and Ago H 1999 *Nature* **401** 572
[70] Hu Y, Churchill H O, Reilly D J, Xiang J, Lieber C M and Marcus C M 2007 *Nat. Nanotechnol.* **2** 622
[71] Wang L J, Cao G, Tu T, Zhou C, Hao X J, Su Z, Guo G C, Jiang H W and Guo G P 2010 *Appl. Phys. Lett.* **97** 262113
[72] Wei D, Li H O, Cao G, Luo G, Zheng Z X, Tu T, Xiao M, Guo G C, Jiang H W and Guo G P 2013 *Sc. Rep.* **3** 3175
[73] Yang C H, Lim W H, Zwanenburg F A and Dzurak A S 2011 *AIP Adv.* **1** 042111
[74] Hayes R R, Kiselev A A, Borselli M G, Bui S S, Croke I I I E T, Deelman P W, Maune B M, Milosavljevic I, Moon J S, Ross R S, Schmitz A E, Gyure M F and Hunter A T 2009 *arXiv*:0908.0173
[75] Xiao M, House M G and Jiang H W 2010 *Phys. Rev. Lett.* **104** 096801
[76] Chen B B, Wang B C, Cao G, Li H O, Xiao M and Guo G P 2017 *Sci. Bull.* **62** 712
[77] Petta J R, Johnson A C, Yacoby A, Marcus C M, Hanson M P and Gossard A C 2005 *Phys. Rev. B* **72** 161301
[78] Studenikin S A, Thorgrimson J, Aers G C, Kam A, Zawadzki P, Wasilewski Z R, Bogan A and Sachrajda A S 2012 *Appl. Phys. Lett.* **101** 233101
[79] Mason J D, Studenikin S A, Kam A, Wasilewski Z R, Sachrajda A S and Kycia J B 2015 *Phys. Rev. B* **92** 125434
[80] Chen B B, Wang B C, Cao G, Li H O, Xiao M, Guo G C, Jiang H W, Hu X D and Guo G P 2017 *Phys. Rev. B* **95** 035408
[81] Hanson R, van Beveren L H, Vink I T, Elzerman J M, Naber W J, Koppens F H, Kouwenhoven L P and Vandersypen L M 2005 *Phys. Rev. Lett.* **94** 196802
[82] Nakajima T, Delbecq M R, Otsuka T, Stano P, Amaha S, Yoneda J, Noiri A, Kawasaki K, Takeda K, Allison G, Ludwig A, Wieck A D, Loss D and Tarucha S 2017 *Phys. Rev. Lett.* **119** 017701
[83] Nowack K C, Shafiei M, Laforest M, Prawiroatmodjo G E D K, Schreiber L R, Reichl C, Wegscheider W and Vandersypen L M K 2011 *Science* **333** 1269
[84] Koppens F H, Buizert C, Tielrooij K J, Vink I T, Nowack K C, Meunier T, Kouwenhoven L P and Vandersypen L M 2006 *Nature* **442** 766
[85] Medford J, Beil J, Taylor J M, Bartlett S D, Doherty A C, Rashba E I, DiVincenzo D P, Lu H, Gossard A C and Marcus C M 2013 *Nat. Nanotechnol.* **8** 654
[86] Medford J, Beil J, Taylor J M, Rashba E I, Lu H, Gossard A C and Marcus C M 2013 *Phys. Rev. Lett.* **111** 050501
[87] Koh T S, Gamble J K, Friesen M, Eriksson M A and Coppersmith S N 2012 *Phys. Rev. Lett.* **109** 250503
[88] Kim D, Shi Z, Simmons C B, Ward D R, Prance J R, Koh T S, Gamble J K, Savage D E, Lagally M G, Friesen M, Coppersmith S N and Eriksson M A 2014 *Nature* **511** 70

[89] Cao G, Li H O, Yu G D, Wang B C, Chen B B, Song X X, Xiao M, Guo G C, Jiang H W, Hu X D and Guo G P 2016 *Phys. Rev. Lett.* **116** 086801

[90] Wang B C, Cao G, Li H O, Xiao M, Guo G C, Hu X D, Jiang H W and Guo G P 2017 *Phys. Rev. Appl.* **8** 064035

[91] Shi Z, Simmons C B, Prance J R, Gamble J K, Koh T S, Shim Y P, Hu X D, Savage D E, Lagally M G, Eriksson M A, Friesen M and Coppersmith S N 2012 *Phys. Rev. Lett.* **108** 140503

[92] Li H O, Xiao M, Cao G, You J and Guo G P 2014 *Physica E* **56** 1

[93] Dyakonov M I and Perel V I 1972 *Soviet Phys. Solid State* **13** 3023

[94] Elliott R J 1954 *Phys. Rev.* **96** 266

[95] Bir G L, Aronov A G and Pikus G E 1976 *Soviet J. Exp. Theor. Phys.* **42** 705

[96] Khaetskii A V and Nazarov Y V 2000 *Phys. Rev. B* **61** 12639

[97] Koppens F H L, Folk J A, Elzerman J M, Hanson R, van Beveren L H W, Vink I T, Tranitz H P, Wegscheider W and Kouwenhoven L P 2005 *Science* **309** 1346

[98] Ono K and Tarucha S 2004 *Phys. Rev. Lett.* **92** 256803

[99] Jelezko F, Gaebel T, Popa I, Gruber A and Wrachtrup J 2004 *Phys. Rev. Lett.* **92** 076401

[100] Rugar D, Budakian R, Mamin H J and Chui B W 2004 *Nature* **430** 329

[101] Xiao M, Martin I, Yablonovitch E and Jiang H W 2004 *Nature* **430** 435

[102] Engel H A and Loss D 2001 *Phys. Rev. Lett.* **86** 4648

[103] Engel H A and Loss D 2002 *Phys. Rev. B* **65** 195321

[104] Laird E A, Barthel C, Rashba E I, Marcus C M, Hanson M P and Gossard A C 2007 *Phys. Rev. Lett.* **99** 246601

[105] Nowack K C, Koppens F H, Nazarov Y V and Vandersypen L M 2007 *Science* **318** 1430

[106] Pioro-Ladrière M, Obata T, Tokura Y, Shin Y S, Kubo T, Yoshida K, Taniyama T and Tarucha S 2008 *Nat. Phys.* **4** 776

[107] Kato Y, Myers R C, Driscoll D C, Gossard A C, Levy J and Awschalom D D 2003 *Science* **299** 1201

[108] Golovach V N, Borhani M and Loss D 2006 *Phys. Rev. B* **74** 165319

[109] Tokura Y, van der Wiel W G, Obata T and Tarucha S 2006 *Phys. Rev. Lett.* **96** 047202

[110] Crippa A, Maur R, Bourdet L, Kotekar-Patil D, Amisse A, Jehl X, Sanquer M, Lavieville R, Bohuslavskyi H, Hutin L, Barraud S, Vinet M, Niquet Y M and De Franceschi S 2018 *Phys. Rev. Lett.* **120** 137702

[111] Salis G, Kato Y, Ensslin K, Driscoll D C, Gossard A C and Awschalom D D 2001 *Nature* **414** 619

[112] Burkard G, Loss D and DiVincenzo D P 1999 *Phys. Rev. B* **59** 2070

[113] Meunier T, Calado V E and Vandersypen L M K 2011 *Phys. Rev. B* **83** 121403